AG-336

9. WALL CORRECTION METHODS FOR DYNAMIC TESTS

AUTHOR R. VOß

9. WALL CORRECTION METHODS FOR DYNAMIC TESTS

9.1 INTRODUCTION

Wind tunnel wall interference in unsteady flow has not been as thoroughly investigated as it has been in steady flow. In the case of unsteady flow, the problem of wind tunnel wall interference is complicated even more by additional parameters describing the time dependent variation of the unsteady flow field. Moreover, other sources of interference such as tunnel wall reflections in the form of acoustic waves, and, as a consequence, wind tunnel resonance, play an important role as well.

Most investigations on unsteady wind tunnel wall interference known so far have concentrated on (harmonically) oscillating lifting systems and bodies undergoing small amplitudes of motion in closed and ventilated wind tunnel test sections. For the case of such motion-induced unsteady flow, a general outline of the problem from a theoretical point of view is given in Ref. [28]. [3] reports on investigations in a small wind tunnel test section with slotted walls and with closed walls. In cases with no different steady pressure distribution between the tests with the different walls, the unsteady results were in a good agreement as well , while for higher transonic Mach numbers both the steady and unsteady results were affected significantly by difference in tunnel walls. Experimental results from systematic wind tunnel interference measurements are reported in [29]. Lambourne [21] reports results of oscillatory wing tests in 4 European wind tunnels. Unsteady interference effects in the smaller tunnels (DRA Bedford, DLR Göttingen) were bigger and led to a suppression of unsteady pressure peaks (due to shock motions) that were clearly present in the larger tunnels (ONERA S2 Modane, NLR HST Amsterdam). The ratios of model span-to-tunnel width were 0.45 and 0.25 for the smaller and bigger tunnels, respectively (see **Figure 1)**. Nevertheless, most unsteady aerodynamic tests are not even performed in tunnels with

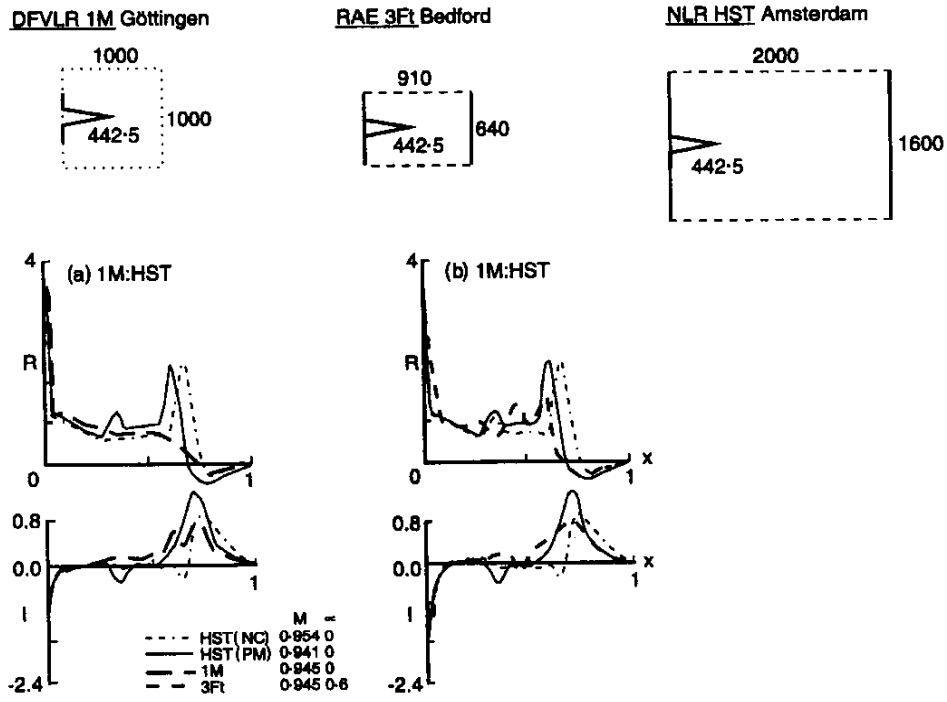

Figure 1 : Results of unsteady measurements in different wind tunnels
(AGARD Tests on the NORA Wing).

stationary adaptation. Unsteady tunnel interferences are neglected, only the vicinity of tunnel resonance is avoided, and the largest ratio of tunnel-to-model size is chosen. But such results become questionable, especially when they are expected to serve for the validation of CFD codes. Meanwhile, these have reached a maturity that demands from validation experiments accuracies of a few percent for unsteady lift and moment coefficients.

Of course, tunnel interference may also affect flutter tests because the critical flutter index (speed or tunnel pressure) is strongly governed by unsteady motion-induced airloads. Lu [25] reports flutter tests with 3 flutter models of a Delta wing of different size but having structural dynamical similarity. Tests in the same wind tunnel have shown significant influence of the model-to-tunnel size ratio on the flutter boundary.

Additional complexity in wind tunnel wall interference arises for rotary balance tests and for oscillatory tests with large support systems. Model support structures have to be massive in order to provide the necessary stiffness while forcing the desired model motion. Large support structures lead to additional strong interferences between the model, support and tunnel walls. While interference between model and tunnel walls is characterised by one lag time for the convection of unsteady waves between the model and tunnel walls, model-support-wall interference (often including separated flow regions) will involve more characteristic time lags. While there is hardly a chance to correct these complicated interference effects, unsteady tunnel interferences for oscillatory 2D and 3D clean wing model tests in sub- and transonic flows have been investigated, modelled and also corrected for during the last years.

With the recent developments of adaptive wind tunnel walls, by which steady wall effects are eliminated or significantly reduced by actively controlling flow near the walls, new possibilities for the correction of wind tunnel wall interference have also emerged for unsteady flow. In the following, the prospects and concepts of experimental and analytical techniques for the correction of unsteady wind tunnel wall effects, appearing with aerodynamic and aeroelastic measurements of oscillating lifting systems and bodies, are presented. First, some fundamental relations of motion-induced unsteady flow fields, basic for a physical understanding and analytical treatment of unsteady flow phenomena, are explained. Then the principal causes of unsteady wind tunnel interference are described and the practicability of adaptive wind tunnel walls to eliminate unsteady aerodynamic wall interference effects in unsteady aerodynamic and aeroelastic wind tunnel model measurements is discussed. Finally, prospective wind tunnel wall corrections for motion-induced unsteady flow, applying steady flow wall adaptation and CFD techniques, are outlined.

9.2 PHYSICAL BASICS OF UNSTEADY WIND TUNNEL INTERFERENCE

9.2.1 CHARACTERISTICS OF MOTION-INDUCED UNSTEADY FLOW FIELDS

The differential equation which governs the inviscid unsteady flow due to small oscillatory perturbations imposed on a steady, uniform flow field is a wave equation. In reference to rectangular co-ordinates, see **Figure 2**, this equation for two-dimensional unsteady compressible flow, generated by an oscillating airfoil, reads as (see [23]):

$$\left(1-M_\infty^2\right)\phi_{xx}+\phi_{yy}-2\frac{M_\infty^2}{U_\infty}\phi_{xt}-\frac{1}{a_\infty^2}\phi_{tt}=0 \qquad (9.1)$$

Here $\phi=\phi\left(x,y,t\right)$ is the time-dependent perturbation velocity potential, U_∞ the velocity of the undisturbed flow, M_∞ the corresponding Mach number and a_∞ the velocity of sound. When the steady free stream Mach number is close to unity, the governing equation for 2D transonic flow in its simplest form reads as:

$$\left(1-M_\infty^2\right)\phi_{xx}-(\gamma+1)\frac{M_\infty^2}{U_\infty}\left[\phi_x^0\ \phi_x\right]+\phi_{yy}-2\frac{M_\infty^2}{U_\infty}\Phi_{xt}-\frac{1}{a_\infty^2}\phi_{tt}=0 \qquad (9.2)$$

where γ denotes the ratio of specific heats. Eq. (9.2) is the time-linearised transonic small perturbation (TSP) equation, where we recognise a non-linear term associated with the steady flow potential ϕ^0 independent of time *t*. The corresponding 3D equation includes an additional term ϕ_{zz}. In the case of harmonic motion of the airfoil,

$$\phi\left(x,\ y,\ t\right)=\phi\left(x,\ y\right)e^{i\omega t} \qquad (9.3)$$

with the co-ordinate transformations
(L = reference length)

$$\bar{x}=\frac{x}{L},\bar{y}=\beta\frac{y}{L},T=\frac{U_\infty}{L},\beta=\sqrt{1-M_\infty^2} \qquad (9.4)$$

and upon introduction of a reduced velocity potential φ, Eq. (9.1) can be transformed into the well-known Helmholtz wave equation:

$$\phi=\varphi^{i\bar{\omega}x}\Rightarrow\varphi_{\bar{x}\bar{x}}+\varphi_{\bar{y}\bar{y}}+\lambda^2\varphi=0 \qquad (9.5)$$

A fundamental solution is:

$$\phi\sim H_0^{(2)}\left(\lambda r\right) \qquad (9.6)$$

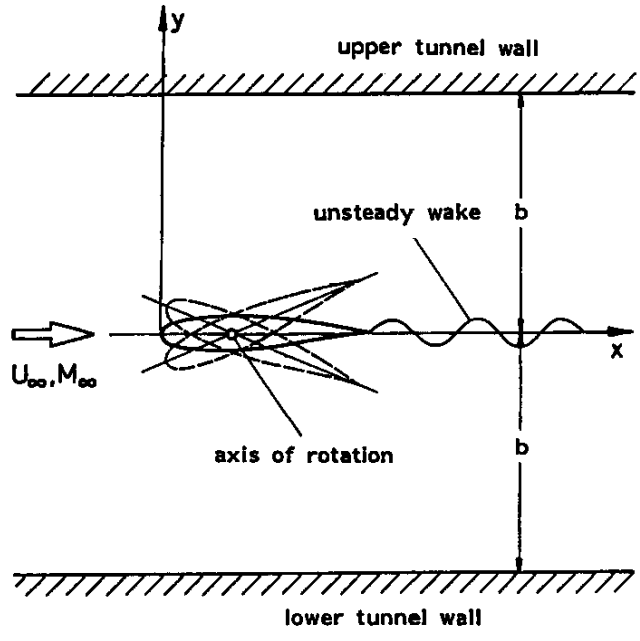

Figure 2 : Oscillating airfoil in a wind tunnel

with *H* denoting the Hankel function of a second kind and order zero, satisfying the Sommerfeld radiation condition and ω = circular frequency, *k* = reduced frequency, λ = reduced wave number; *r* denotes the hyperbolic distance between the transmitting point $\left(\xi,n\right)$ and control point (x, y) of the flow field.

$$k=\frac{\omega L}{U_\infty},\lambda=\frac{kM_\infty}{\beta^2},\varepsilon=\lambda M_\infty \qquad \left(r=\sqrt{(\bar{x}-\bar{\varsigma})^2+(\bar{y}-\bar{\eta})^2}\right) \tag{9.7}$$

Hence, the unsteady part of the flow field of a harmonically oscillating airfoil may be represented by a superposition of perturbation sources which move with the basic flow velocity U_∞ and propagate in the form of waves with the velocity of sound a_∞, thus exhibiting a waviness in the flow field dependent on the parameter λ and on the mode of oscillation as well. As a typical example, **Figure 3** illustrates the motion-induced unsteady flow field of an oscillating airfoil in 2D compressible flow, where φ' denotes the real part (in phase with the oscillating airfoil) and φ'' the imaginary part (90 degrees out of phase) of the unsteady velocity potential. It can be seen that this unsteady flow field is by far more complicated than the steady flow field of an airfoil at rest.

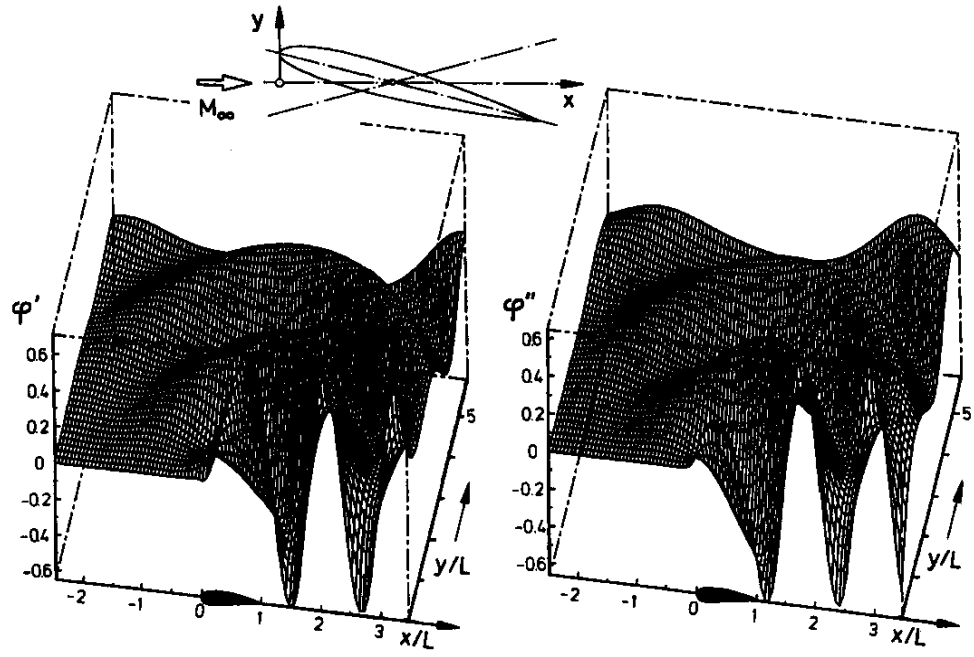

Figure 3 : Motion-induced unsteady flow field (complex unsteady potential) of an airfoil in harmonic pitch oscillation around 42.5% chord axis (φ' = real , φ'' = imaginary part)

For transonic flows, the oscillatory behaviour of motion-induced unsteady 2D and 3D flow fields was thoroughly investigated in [38]. Unsteady flow fields induced by small amplitudes may be modelled by singularity distributions, whose disturbances propagate as nearly plane waves through a non-homogeneous steady flow field. This propagation is described by a nonhomogeneous Helmholtz equation, which is derived from Eq. (9.2).

$$\varphi_{\bar{x}\bar{x}}+\varphi_{\bar{y}\bar{y}}+\lambda^2\varphi=\left(\frac{\partial}{\partial\bar{x}}+i\varepsilon\right)\left(\frac{(\gamma+1)M_\infty^2}{\beta^2}\phi^0{}_{\bar{x}}\left(\varphi_{\bar{x}}+i\varepsilon\varphi\right)\right) \tag{9.8}$$

The right-hand side of (9.8) models the effects of nonuniform steady transonic flow on the propagation of disturbances. Of main importance are the curvature and density of acoustic rays, which are properties directly related to the transonic influence and to the density of disturbance energy. **Fig. 4** shows a typical result of propagation in a 2D transonic flow field. Only in the near field of the airfoil, transonic effects

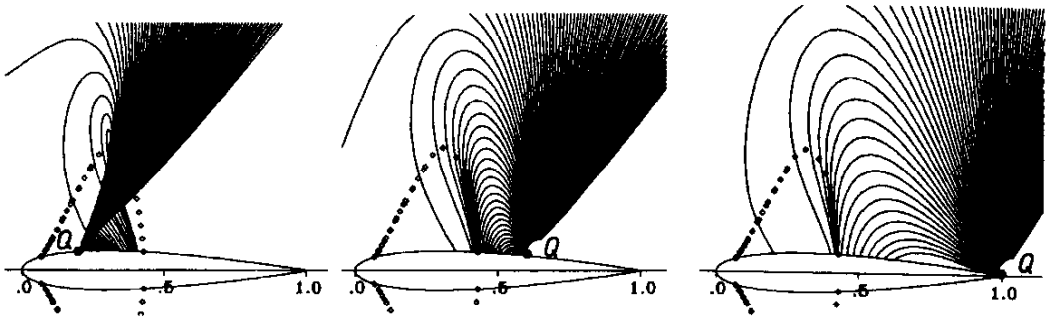

Figure 4 : Propagation of acoustic disturbances (rays) in a transonic flow field
(NACA 0012, $Ma_\infty = 0{,}79$) ◊◊◊◊◊ : boundary of local supersonic bubbles

significantly change the ray curvature and ray density compared to the behaviour in a homogeneous flow (straight rays with uniform density). Note that upstream disturbances propagate themselves in such a manner that they are bent around the shock, which forms the downstream boundary of the local supersonic region. The ray density is very large near the shock and very small in the supersonic region. This corresponds to large and small values of disturbance energy. Rays reaching the tunnel walls are not significantly affected by the transonic effects as long as local supersonic regions do not extend close to the walls. Then the flow near the walls may be fully described by the linear theory because all disturbances from the airfoil reaching the walls propagate themselves, nearly unaffected by the local supersonic bubble.

9.2.2 WIND TUNNEL INTERFERENCE EFFECTS IN UNSTEADY FLOW

From the practical point of view, the most important types of motion-induced unsteady flow fields in a wind tunnel arise from forced or self-excited (flutter) oscillations of the model. In such wind tunnel investigations the unsteady aerodynamic data of main interest are the magnitude and phase of the motion-induced unsteady pressures. For instance, for an airfoil performing pitching oscillation of amplitude $\Delta\alpha$ about a mean incidence α_0, the wall interference effects on magnitude and phase of the unsteady pressures can be considered under the following headings :

- steady effects on the flow for the mean incidence α_0 ,
- quasi-steady effects in context with the time-dependent kinematic flow conditions for all changes of incidence within the range $(\alpha_0 - \Delta\alpha) < \alpha < (\alpha_0 + \Delta\alpha)$,
- unsteady effects on the manner in which the magnitude and phase of the motion-induced unsteady pressure vary with frequency in context with the unsteady wake.
- unsteady effects in compressible flow from acoustic interference

Hence, the requirements for the avoidance of wind tunnel wall interference effects in unsteady tests are:

- correct (undisturbed) base flow and correct steady perturbations,
- absence of any additional unsteady effects,

i.e., an unsteady process may be directly affected by steady flow wall interference as well as by the purely unsteady sources of interference, as demonstratively shown in [22]. The principal causes of unsteady tunnel interference - in addition to the well known steady interference effects, such as wall constraint, shock wave reflection in transonic flow and wall boundary layers - are (see **Figure 5**) :

- unsteady effects of wall constraint,
- reflection by the walls of model generated acoustic disturbances, and - as a consequence -
- acoustic wind tunnel resonance,
- distortion of the oscillatory wake of the model by other tunnel deficiencies,
- inherent tunnel flow fluctuations,
- wing support interference.

In [7], wall effects on a transient motion of an airfoil in incompressible flow (stepwise change in angle of attack) is theoretically investigated. This is of importance for tests in response to control deflections. The unsteady development of lift strongly depends on the relative model size, as well as on the type of tunnel walls. Lift is built up faster for open walls than for closed ones and the influence of the relative model

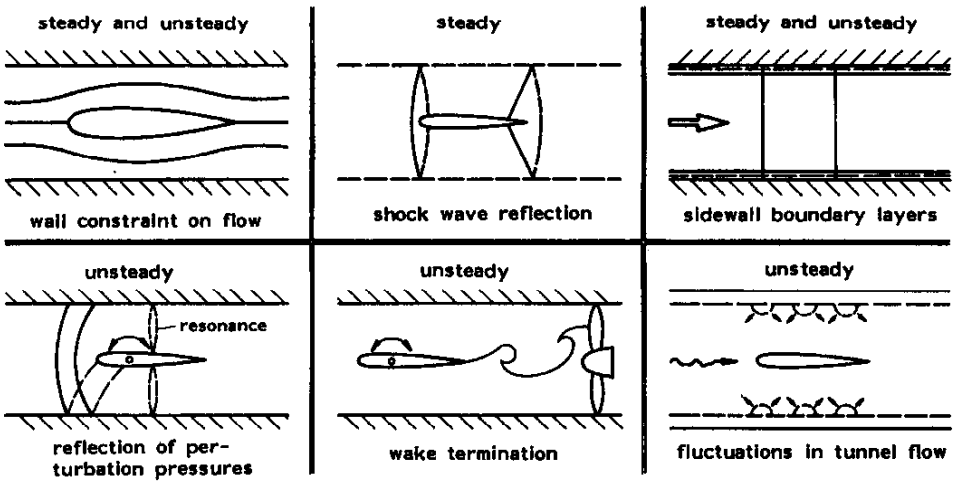

Figure 5 : Principal causes of wind tunnel interference

size is more significant for open walls.

Since a clear understanding of these unsteady wind tunnel interference effects is a basic concern for the application of adaptive wall concepts and the development of correction methods, they will be discussed in more detail in the following. Corrections for unsteady effects of wall constraint - excluding transonic flow- in tunnels having well-defined wall boundary conditions can readily be obtained from theoretical investigations. The corresponding boundary conditions for open and closed (solid) wind tunnel walls can easily be established, see [28], but it is difficult to obtain estimations for ventilated wind tunnel walls because of mathematical uncertainties about the boundaries. For two dimensional airfoils oscillating in sub- and supersonic flow several of such analytical unsteady wall correction techniques have already been elaborated.

In a free atmosphere an oscillating model would leave behind an oscillating wake, the vorticity distribution of which is consistent with the unsteady flow at the model. If this wake is affected by a tunnel shock wave in a tunnel, driving fan, a near tunnel corner, or a support system, the unsteady aerodynamic loading at the model may be notably influenced. There are reasons to suggest that this source of unsteady interference is of considerable importance in certain special cases of flow speed and less important in transonic flow.

Finally, various types of flow fluctuations, often collectively described as tunnel noise, can have several unwanted effects, particularly in aeroelastic model investigations. One of the principal sources of noise in

transonic tunnels is the flow over ventilated walls. It is possible to reduce the noise from these walls by covering the perforations with gauze cloth and to apply sound-absorbing material to the tunnel walls, as shown in [26].

9.2.3 UNSTEADY WIND TUNNEL WALL BOUNDARY CONDITIONS

Pressure in a flow field with small unsteady perturbations of an undisturbed homogeneous mean flow fulfils the following equation

$$c_p = -\frac{2}{u_\infty}\frac{d\phi}{dt} = -\frac{2}{u_\infty}\left(\frac{\partial}{\partial t} + u_\infty \frac{\partial}{\partial \bar{x}}\right)\phi \tag{9.9}$$

with the pressure coefficient

$$c_p = \frac{\left(p - p_\infty\right)}{0.5\,\rho u_\infty^2} \tag{9.10}$$

In the following, the disturbance normal velocity component v with respect to the walls is important

$$\frac{v}{u_\infty} = \frac{\partial \phi}{\partial n} = \pm\frac{\partial \phi}{\partial y} \qquad \textit{with} \quad n = \pm y \quad \textit{for upper or lower wall} \tag{9.11}$$

In the following, it is assumed that the flow field may be modelled by a mean steady flow and an unsteady harmonic perturbation

$$\phi\left(x,y,t\right) = \phi^{0}\left(x,y\right) + \phi\left(x,y\right)e^{i\omega t} \tag{9.12}$$

While numerical computations of unsteady flow fields assume nonreflecting far field boundary conditions at outer boundaries (Sommerfelds radiation condition), tunnel walls have to be taken into account by special conditions.

Closed (solid) walls: vanishing normal velocity component at the walls for both steady and unsteady flow component

$$v = 0 \Rightarrow \frac{\partial \phi}{\partial n} = \phi_n = 0 \tag{9.13}$$

Open walls (free jet): vanishing pressure disturbances $\left(p = p_\infty\right)$ at the walls

$$\left(c_p = \left(\phi_x + ik\phi\right) = 0 \Rightarrow \phi\left(x\right) = \phi\ \left(-\infty\right)e^{-ik\left(x-\infty\right)}\right) \Rightarrow \phi = 0 \tag{9.14}$$

taking into account that the unsteady disturbance potential vanishes for infinite upstream position.

Ventilated walls: The two extreme conditions of closed and open walls yield opposite interference effects. While closed walls increase lift, open walls decrease the free air value of lift coefficient. The ventilated walls yield values between the two extreme wall types. In the following, the model is located at $z = 0$ midway between two (upper and lower) tunnel walls $\left(z = \pm b\right)$

Porous (perforated) walls:

$$\text{viscous} \quad \text{effect} \quad Zv = \frac{c_p}{2} \Rightarrow \phi_x + ik\phi + Z\phi_n = 0 \tag{9.15}$$

$$\left(\frac{\partial}{\partial x} + ik\right) c_p(x, \pm b) \pm Z \frac{\partial}{\partial y} c_p(x, \pm b) = 0 \tag{9.16}$$

with a complex porosity factor: $Z = R + iS$, $R = 1/P$ (resistance) and S reactance

Slotted walls: normal flow with velocity v through the walls is described by momentum equation

$$\rho_\infty \frac{dv}{dt} = \nabla p = \frac{(p - p_\infty)}{K} \tag{9.17}$$

with a slot parameter K (dimension length). This approach yields

$$\phi + K\phi_n = 0$$

$$c_p(x, \pm b) \pm K \frac{\partial}{\partial y} c_p(x, \pm b) = 0 \tag{9.18}$$

Here the limiting cases of $K = 0$ and $K = \infty$ describe the open jet and solid walls, respectively.

9.2.4 Acoustic Interference and Tunnel Resonance

In compressible flow, the reflection of acoustic disturbances from wind tunnel walls and their return to the model is a crucial unsteady interference problem. As shown in the previous section, an oscillating model generates unsteady pressure disturbances in the form of travelling acoustic waves which propagate outwards in the tunnel. After being reflected from the walls, these disturbances return to the model, causing additional pressure changes there. This is in contrast to the Sommerfeld far field radiation condition, which requires a reflection-free propagation of disturbances to infinity in free atmosphere.

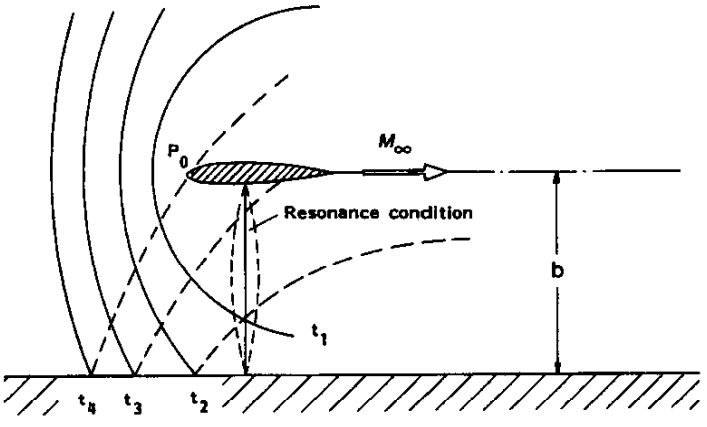

Figure 6 : Positions of wave front from a disturbance at P_0 and reflection of acoustic waves from a wall

Figure 6 shows an airfoil in 2D subsonic flow and the wave fronts from an acoustic disturbance in a uniform flow. It is seen that the velocity of propagation of the pressure disturbance from a point P_0 in the direction normal to the walls is $a_\infty^2 - U_\infty^2$, and the time needed for the disturbance to be reflected by the wall and return to P_0 is :

$$\Delta t = 2\frac{b}{\sqrt{a_\infty^2 - U_\infty^2}} = 2\frac{b}{\beta a_\infty} \tag{9.19}$$

where b is the distance to the wall. The attenuation of the disturbance by the time it returns to the source will depend on the distance travelled in the moving air which is

$$a_\infty \Delta t = 2\frac{b}{\beta} \tag{9.20}$$

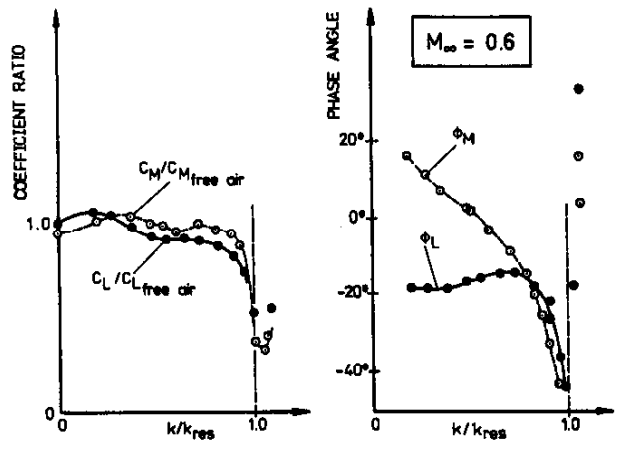

Figure 7 : Resonance in a solid wall test section (adapted from Fromme)

Thus the reflected wave when it returns will be weaker (by natural damping), the higher the Mach number. When a disturbance from the oscillating airfoil is reflected from the tunnel wall back to the wing with such a phase relationship that it reinforces or cancels out a succeeding disturbance and, hence, the pressure changes currently occurring on the model, the most severe unsteady wall interference problem happens, as first described in [33], [1], [14] and experimentally verified in [33], see **Figure 7**. At this resonance condition, the disturbances emitted from an oscillating wing and reflected by the walls form a standing wave pattern. For solid walls, that do not change the phase of the wave on reflection, the resonance circular frequency is :

$$\omega_n = (2n-1)\pi\, U_\infty \frac{\beta}{M_\infty}\frac{1}{2b} \qquad n = 1,2,\ldots. \tag{9.21}$$

For open jet boundaries the phase change on reflection is π, so that

$$\omega_n = 2n\pi\, U_\infty \frac{\beta}{M_\infty}\frac{1}{2b} \qquad n = 1,2,\ldots. \tag{9.22}$$

For a tunnel with ventilated walls, theoretical expressions for resonance frequencies depending on wall porosity, depth of plenum chamber and Mach number are given in [26]. In the case of resonance, where the disturbances form a standing wave pattern, the normal velocity has a maximum amplitude and the pressure has a node, i.e. is of zero amplitude at the position of the oscillating airfoil. Accordingly, the unsteady airloads on the oscillating airfoil will vanish at resonance. Whereas for incompressible flow $\left(M_\infty \to 0\right)$ there is no tunnel resonance - the resonance frequency decreases with increasing Mach number - and since it tends to zero as $\left(M_\infty \to 1\right)$, the predicted resonance frequency must coincide with a test frequency for some intermediate Mach number which causes dramatic changes in the magnitude and phase of the unsteady lift on the oscillating model.

The same expressions derived here for 2D tunnels are valid for tunnels with quadratic test sections.

The lowest value for resonance frequency for a quadratic test section are :

$$\omega_n = n_1\, 2\pi\, U_\infty \frac{\beta}{M_\infty}\frac{1}{2b} \tag{9.23}$$

The value of the parameter n_1 equals 0.5 or 1.0, for closed walls $\left(n_1 = 0.5\right)$, and open walls $\left(n_1 = 1.0\right)$, respectively.

For cylindrical test sections with closed walls the value of the lowest resonance frequency was derived in [33] :

$$\omega_n = n_2 U_\infty \frac{\beta}{M_\infty} \frac{1}{R} \tag{9.24}$$

with $(n_2 = 1.84)$, R = radius of test section.

For ventilated walls the resonance frequencies are given by

$$\omega_n = 2\lambda_n b U_\infty \frac{\beta}{M_\infty} \frac{1}{2b} \tag{9.25}$$

Their values depend on Mach number, tunnel size, wall opening ratio and plenum depth. They are derived from the tunnel wall boundary conditions in chapter 2.3 by decomposition of the unsteady disturbance pressure field into plane waves propagating in the mean flow direction and the transverse direction. Reduced frequency values of resonance conditions depend on Mach number and eigenvalues λ_n of the tunnel section. For detailed derivation see [28].

For slotted walls the eigenvalues depend on the slot parameter K via a transcendental equation: The eigenvalues satisfy the inequalities

$$\lambda_n K + \tan(\lambda_n b) = 0 \tag{9.26}$$

The eigenvalues satisfy the inequalities

$$\left(n - \frac{1}{2}\right)\pi \le \lambda_n b < n\pi \tag{9.27}$$

Again, the limiting lower and upper bounds represent values for closed and open walls, respectively.

For porous walls expressions for resonance frequencies were derived by Mabey [1980], (also see [28]) using the corresponding boundary condition for porous walls of chapter 2.3, but neglecting the reactance, thus approximating $Z = iS$. This yields

$$\lambda_n b = \operatorname{atan}(-S\beta M_\infty) + n\pi \tag{9.28}$$

with the limiting cases $S = \infty$ and $S = 0$ for closed walls and open jet walls respectively.

Fortunately, at higher Mach numbers, there are influences to reduce these effects. Even for strong reflections from solid walls, the effective air distance increases with Mach number and the reflections thus become more attenuated. Also, the reflected disturbances travel more with the flow than across it, see **Figure 6**. Furthermore, for transonic conditions, when resonance frequencies are low enough, the (adapted) walls in typical transonic wind tunnels are perforated or slotted and the reflections are thus more diffuse and attenuated. Thus the strong phenomenon of tunnel resonance is milder in transonic flows.

9.3 WALL ADAPTATION FOR DYNAMIC TESTS

From the preceding explanations we have seen that the following wind tunnel interference effects, due to an unsatisfactory test environment, are of main concern in unsteady aerodynamic and aeroelastic experiments with oscillating models:

1. interference of the steady base flow field by steady wall constraints, including shock wave reflections in transonic flow,
2. interference of the (superimposed) motion-induced unsteady flow field by wall constraints,
3. reflection of the model-generated acoustic disturbances by the walls,
4. acoustic tunnel resonance in the test section.

With regard to the application of adaptive wind tunnel wall concepts to eliminate or significantly reduce these wall interference effects in unsteady flow measurements, the following statements can be made :

9.3.1 STEADY WALL ADAPTATION

The practicability and feasibility of wall adaptation for steady flow have already been successfully demonstrated.

The elimination or at least reduction of unsteady wind tunnel wall interference by means of adaptive walls seems to be extremely difficult to realise. The feasibility of unsteady wall adaptation has not yet been demonstrated. However, since unsteady aerodynamic processes are also affected by steady wall interferences, particularly in the transonic flow regime, the avoidance of steady flow wall effects by the application of steady flow wall adaptation will also significantly improve the results of unsteady wind tunnel measurements, as demonstrated by Kuczka [18] for the "Standard Dynamics Model" (SDM) shown in **Figure 8**. He obtained some satisfactory agreements between results from a tunnel with steady adapted closed walls and with results from tunnels with perforated walls for the in-phase component of unsteady lift and moment coefficients. However, the corresponding out-of-phase components disagree, even for low reduced frequencies. They are especially affected by reflections of model-generated disturbances from the walls, because they are, e.g., smaller than the in-phase components. In addition, the wall reflected disturbances are phase-shifted to the model oscillations.

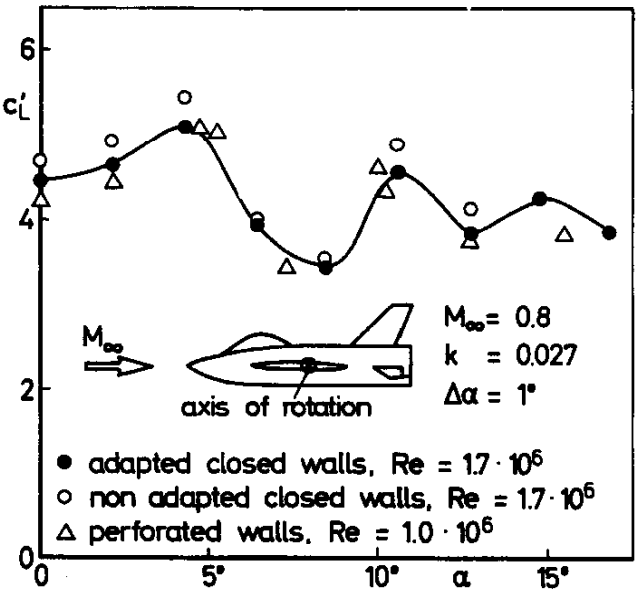

Figure 8 : In-phase component CL' of unsteady lift coefficient of the oscillating SMD model with and without tunnel wall adaptation (adapted from Kuczka)

9.3.2 PASSIVE ADAPTIVE UNSTEADY WALLS

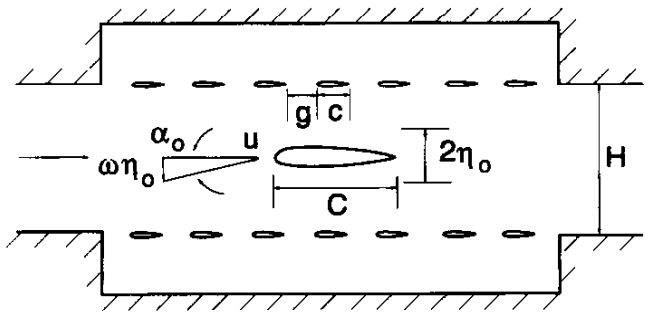

Figure 9 : Principle of airfoil slatted wind tunnel section (adapted from Kong)

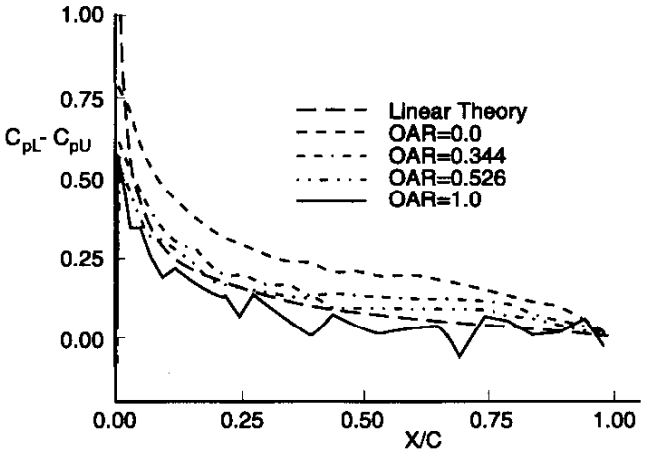

Figure 10 : Measured unsteady pressure distribution for different wall opening area ratios. (adapted from Kong)

In addition to steady adaptation, another promising procedure has shown to be the use of special partly open walls, namely airfoil-slatted tunnel walls. Kong [19] shows that this type of walls avoids the disadvantages of flow separation often appearing with slotted walls.

An opening area ratio parameter, *OAR = g/(c+g)*, see **Figure 9**, with a value of 0.6, has shown to be most successful in eliminating unsteady wall interference. **Figure 10** shows that this OAR provides the best agreement of measured unsteady pressure distributions with free air results. **Figure 11** compares the ratio of measured and analytical free air results for unsteady lift and moment coefficients. The results of tests with different ratios of model- to-tunnel size C/H = 0.333 and 0.667 and of different reduced frequencies for a subsonic oscillating airfoil in plunge motion show that the optimum desired value 1 is achieved with OAR = 0.6 again, for all parameter combinations, thus providing a calibrated value for all tests in this tunnel. This promising method has yet still to be validated for transonic tests as well.

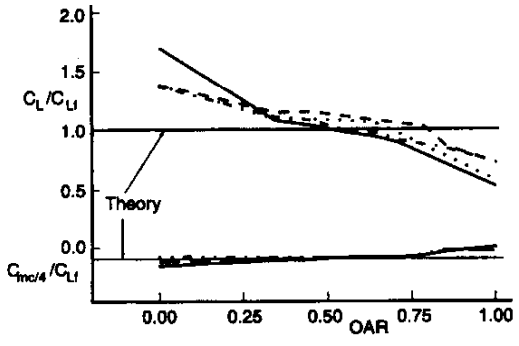

Symbol	C/H	k	$\overline{\alpha}_0^0$	Re · (10)$^{-5}$
- - - - -	0.333	0.52	0.62	2.5
- - · - -	0.333	0.52	0.31	2.5
— — —	0.333	0.37	0.44	2.5
- · · - · ·	0.333	0.37	0.22	2.5
———	0.667	0.48	2.16	7.3
· · · · · · ·	0.667	0.48	1.44	8.0
— - — -	0.667	0.28	0.82	8.0

k = reduced frequency
Re = Reynolds number
$\overline{\alpha}_0^0$ = amplitude of α_0

Figure 11 : Measured unsteady lift and moment coefficients for different wall opening area ratios and different reduced frequencies

9.3.3 ACTIVE ADAPTIVE UNSTEADY WALLS

It is clear that steady adaptation can remove a significant amount of interference effects on unsteady results (see point 1 in chapter 2.2). The effects mentioned in points 2 and 3 may be only cancelled by adaptive walls if a time-dependent adaptation is applied. This has not been done yet. So only the practicability of such a method may be studied theoretically or numerically.

Unsteady wall adaptation can be realised, at least theoretically, in the same way as with steady flow conditions. However, enormous technical effort is mandatory even for 2D measurements. Unsteady wall adaptation would require oscillatory moving flexible walls, where an unsteady motion of the wall contours would depend on the frequency and the vibration mode of the model, on the model amplitude of oscillation and on certain phase relationships with respect to the motion of the model. Streamlining algorithms for such a nonstationary wall adaptation, even for the simplest case of non-flexible (rigid body) oscillations of the model, would be very difficult to establish. They demand unsteady pumping tunnel walls governed by the unsteady varying stream surface contour. For imposed prescribed unsteady motions this might be feasible by pre-tests computing the wall contours in advance. It seems unlikely that point 4 (tunnel resonance) may be cancelled at all. Unsteady wall adaptation may be best realised for low-frequency flow fields because then acoustic interference is small and the speed of the wall contour changes is low.

In [6] a study on unsteady wall adaptation is carried out for 2D low-frequency oscillating airfoils in transonic flow. A CFD code based on the unsteady Euler equations is used to compute the unsteady airloads on the oscillating model in the presence of solid tunnel walls. The exact time dependent wall contours like the airfoil contour are precisely modelled by the computational grids. The parameter ratios of model-to-tunnel size, reduced frequency and Mach number are varied. Three different tunnel wall adaptation concepts (all based on the streamlining of the wall contours) with increasing degree of complexity are tested, namely:

1) steady wall adaptation for the mean flow field,
2) quasisteady synchronisation of wall adaptation (e.g. harmonically deforming walls between steady adapted wall contours obtained for maximum and minimum motion amplitude,
3) unsteady synchronisation by choosing wall contours compatible with streamlines for a time dependent vortex at the position of the model and compatible with the measured unsteady lift of the model.

Results for unsteady airloads obtained with these different wall adaptation procedures are presented in **Figure 12,** showing that the quasisteady adaptation for subsonic flow is sufficient while transonic flow

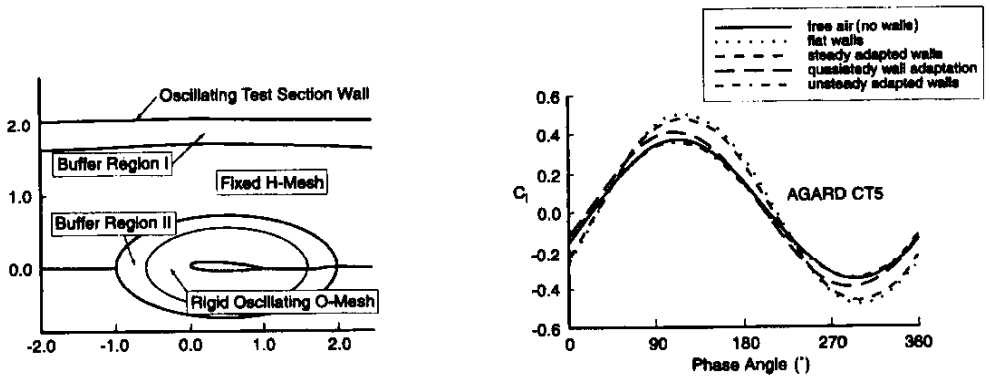

Figure 12 : Numerical simulation of unsteady wall adaptation strategies (adapted from Chang)

demands at least an unsteady synchronisation of the wall contours. There is still the question if the unsteady lift dependent synchronisation is sufficient for higher frequencies since significant time lags between streamline contour at the wall positions and the instantaneous lift will arise.

Summarising, steady wall adaptation is a necessary prerequisite for obtaining interference-free unsteady results. But this is not sufficient at least for transonic flows and higher frequencies, and one somehow has to correct the residual unsteady interference effects. An unsteady wall adaptation procedure working for different Mach numbers, frequencies and model motions seems difficult to realise. Sophisticated correction methods based on mathematical models and CFD computations offer a more promising approach instead. In order to model unsteady wall boundary conditions with such methods, unsteady pressure data should also be measured at the walls. Indeed, the application of adaptive walls to minimise interference from steady flow wall constraints, together with the application of CFD-techniques which take into account the unsteady wall pressure data from experiments to describe precise wall boundary conditions, is most promising in deriving corrections for wind tunnel wall interferences in unsteady flow. Prospects and concepts for such hybrid wind tunnel wall correction techniques are outlined in the following.

9.4. MODELLING OF UNSTEADY WALL INTERFERENCES AS A BASIC FOR CORRECTION METHODS

Analytical predictions of wall effects on unsteady pressures and airloads require the precise knowledge of the wall boundary conditions. Only three types of boundary conditions are well defined, namely those of solid (closed) walls, free jet and of prescribed unsteady wall pressure distributions (known from experiments). Porous and slotted walls can be simulated only approximately by mixed boundary conditions including free parameters. As wind tunnel tests with oscillating models are primarily performed for aeroelastic purposes, wind tunnel interference effects have to be studied within a wide range of Mach numbers, oscillation modes and reduced frequencies. For 2D subsonic flow in one of the first systematic analytical investigations on wind tunnel wall effects, Bland [5] derived an integral equation relating the downwash w (prescribed by the harmonic motion of the airfoil) to the induced unsteady pressure jump δp at the airfoil :

$$w(x) = \int_0^1 K\left(\bar{x} - \bar{\zeta}, M_\infty, k\right) \delta p\left(\bar{\zeta}\right) d\bar{\zeta} \tag{9.29}$$

This is an extension of Possio's integral equation [31], [13], which is valid for unbounded free air conditions. Bland derived a rather complicated corresponding kernel K, including tunnel wall boundary conditions to be automatically fulfilled on infinitely extended walls in the general form:

$$p \pm c_w \frac{\partial p}{\partial y} = 0 \, at \; y = \pm b \left\{ \begin{matrix} upper \\ lower \end{matrix} \right\} walls \tag{9.30}$$

where c_w denotes a specific wall parameter. The limiting cases of solid walls and free jet condition are included:

$$c_w = 0 \rightarrow p = 0 \rightarrow \varphi = 0 \left(free \quad jet \right) \tag{9.31}$$

$$c_w = \infty \rightarrow \frac{\partial p}{\partial y} = 0 \rightarrow \frac{\partial \varphi}{\partial y} = 0 \left(closed \quad wall \right)$$

Thus the effects of ventilated walls are described by certain values of C_w, but its dependence on the type of walls, their opening ratio and perhaps Mach number and reduced frequency is unclear and would have to be systematically studied by comparing computations and experiments. Bland's method was completed by Fromme and Golberg [11], []13], who improved the numerical performance of the solution method and extended it to general oscillation modes, including control surfaces. They obtained results clearly showing the unsteady wall effects, especially the sharp drops in magnitude of the loads and their phase jumps in the case of tunnel resonance, see **Figure 13**. Wall effects are significant in the whole frequency regime and wall-influenced loads are bigger/smaller than the corresponding free air value for closed/open walls, which is well known for steady or quasisteady flow. In particular, the strong changes in phase deserve special attention. This analytical method provides exact reference results, but it is restricted to 2D flows and to the regime of linear compressibility, i.e. constant Mach number in the whole flow field, and thus subsonic flow. It hardly appears possible to extend it to 3D or transonic flow.

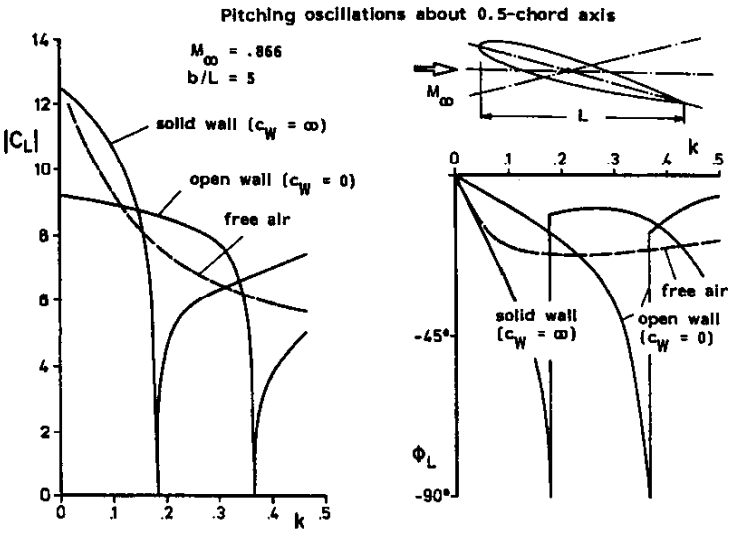

Figure 13 : Lift coefficient (magnitude and phase) of an airfoil performing harmonic pitch oscillations around a 50% chord axis (adapted from Fromme)

Another method of indirectly modelling the walls is the method of images. In an integral equation for the solution of the boundary value problem of an oscillating model the influence of solid tunnel walls is taken into account by an image of the model located on the other side of the wall, the wall being a mirror plane. This single image is sufficient in the presence of only one wall.

In the presence of upper and lower walls, images mirrored by both walls have to be taken into account, each of which has to then be mirrored again by the other wall as well, a procedure yielding an infinite series of images with increasing distances across all walls. This method has been thoroughly elaborated by Mabey [27] for ventilated walls as well. The rather complicated procedure of summing up contributions of the infinite series, each element of which is representing a model either by vortices or by more precise panel distributions, may be simplified, because often a small finite number of images is sufficient. This is demonstrated in

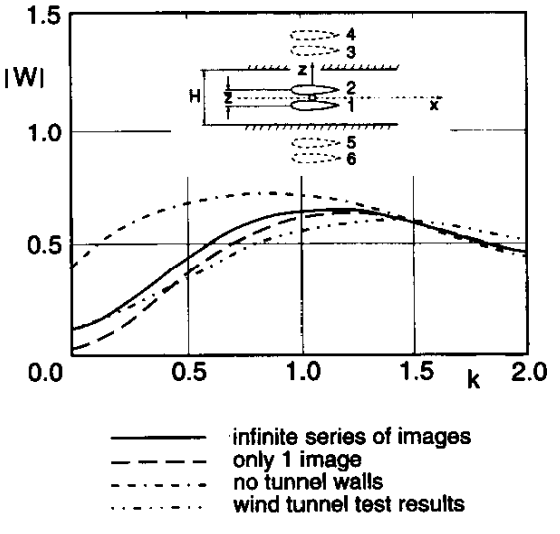

Figure 14 : Results of modelling unsteady tunnel wall effects by methods of images (adapted from Laschka). Induced unsteady downwash velocity behind an oscillating airfoil system in a wind tunnel (H = 6.5, $\bar{z}$ = 3.5, k = reduced frequency)

Figure 14, adapted from [24]. For a gust generator with two oscillating airfoils the induced normal velocity component *w* at the tunnel centre line *z = 0* at a position downstream of the gust generator *(x = 5)* is shown. |*w*| denotes the magnitude of the downwash velocity *w*, normalised by the amplitude of the airfoil oscillation. With respect to the measured results, the wall interference effects are modelled with sufficient accuracy by just one image. Note that, for reduced frequency *k = 0* (quasisteady condition), |*w*| is not zero because w (k=0) is defined as the difference between the steady *w* values at the maximum and minimum incidence of the airfoils (normalised by $\Delta\alpha$).

The advantage of these two methods, namely the reformulation of integral equation kernels and method of images, lies in the fact that tunnel walls are taken precisely into account, being infinitely extended upstream and downstream. Thus, the walls do not have to be directly modelled by singularities (like the model).

However, these methods will hardly be able to predict details of the wall affected pressure distribution at the model, because a derivation of modified 3D kernels seems very complicated, while the complexity of infinite series of images can be evaluated numerically only with a rough representation of the wing and its images, like simple horseshoe vortices.

The following numerical approach, see [36] and [39], is more flexible. It is also based on the 2D linear equation, but may be extended straightforward to 3D and transonic flows. Within the framework of unsteady linearised theory (small oscillation amplitudes) the position of the airfoil, its wake and the walls (even if curved for steady adaptation) may be assumed to be approximately parallel to the x-axis (freestream direction of the wind tunnel). The airfoil is located midway between the tunnel walls, a distance *b* away from them. Then this 2D boundary value problem can be solved by application of Green's theorem:

$$\varphi(\bar{x},\bar{y}) = \oint_C \left(\psi \frac{\partial \varphi}{\partial n} - \varphi \frac{\partial \psi}{\partial n}\right) ds = 0 \qquad with \quad \psi = \frac{1}{4i} H_0^{(2)}(\lambda r) \tag{9.32}$$

Green's function ψ satisfies the 2D Helmholtz-equation together with Sommerfeld's far field radiation condition for free air. For 3D problems Green's corresponding function reads as $\psi = \frac{e^{i\lambda r}}{r}$. The integration contour *C* and the integration path *s* run along the boundaries of the control volume and along those boundaries where φ is discontinuous, see **Figure 15**.

$$\varphi = \int_0^\infty \left(\delta\varphi\psi_{\bar{\eta}} + \delta\varphi_{\bar{\eta}}\psi\right)_{profile} d\zeta - \int_{-\infty}^{\infty} \left(\left(\psi\varphi_{\bar{\eta}} + \varphi\psi_{\bar{\eta}}\right)_{lo}\right) d\zeta + \int_{-\infty}^{\infty} \left(\left(\psi\varphi_{\bar{\eta}} - \varphi\psi_{\bar{\eta}}\right)_{up}\right) d\zeta \tag{9.33}$$

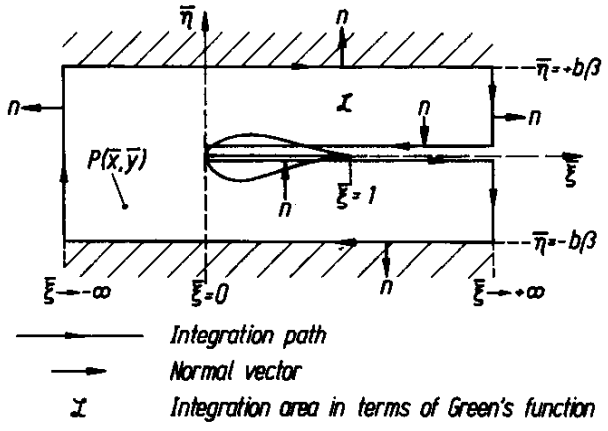

Figure 15 : Integration path and area for the unsteady flow problem of an oscillating airfoil in a wind tunnel

For free air conditions, the infinite boundaries give vanishing contributions; only airfoils and wake contour lines have to be taken into account. For wind tunnel flows the integration path also runs along the tunnel walls. As a final result, one obtains an analytical relationship between the downwash *w* at the airfoil, which is prescribed by the airfoil's oscillatory motion, and the unsteady potential function value *f* and the normal unsteady velocity component *g*, both at the walls :

$$w = \frac{\partial \varphi}{\partial \bar{y}} \quad (profile), \qquad f = \varphi \quad (walls), \qquad g = \frac{\partial \varphi}{\partial \bar{y}} \quad (walls) \tag{9.34}$$

For *f* and *g* indices "up" and "lo" denote values at the upper or lower tunnel wall, respectively. The downwash in the presence of tunnel walls is governed by the following relation

$$\begin{aligned} w(x) &= -\int_0^\infty \delta\varphi(\zeta)\psi_{\bar{\eta}\bar{\eta}}(x-\zeta,0)\,d\zeta \\ &-\int_{-\infty}^{\infty}\left(g^{up}(\zeta)\psi_{\bar{\eta}}(x-\zeta,b) - g^{lo}(\zeta)\psi_{\bar{\eta}}(x-\zeta,b)\right) \\ &-\int_{-\infty}^{\infty}\left(f^{up}(\zeta)\psi_{\bar{\eta}\bar{\eta}}(x-\zeta,b) - f^{lo}(\zeta)\psi_{\bar{\eta}\bar{\eta}}(x-\zeta,b)\right) \end{aligned} \tag{9.35}$$

Similar relations are derived for *f* and *g* on the walls, see [39]. If the integral operators are expressed by aerodynamic influence coefficients *A, B, C* etc., the final system reads :

$$\begin{aligned} w &= A\delta\varphi + A_1 f + A_2 g \\ f &= \left(B_0\right)^{(-1)}\left(B\delta\varphi + B_1 g\right) \\ g &= \left(C_0\right)^{(-1)}\left(C\delta\varphi + C_1 f\right) \end{aligned} \tag{9.36}$$

These equations relate the downwash distribution *w* to an unknown dipole distribution $\delta\varphi$, which provides the unknown pressure jump at the airfoil by taking the unsteady flow values *f* and *g* at the wind tunnel walls into account. For the numerical solution the wing profile and the walls are divided into line elements (panels) on which *w*, $\delta\varphi$, *f*, *g* are approximated as constants. The dipole strength in the wake is approximated by the values near the trailing edge and by use of the Kutta condition. Since the unsteady potential function, especially downstream of the airfoil, decreases only slowly, see **Figure 3**, the control volume of the integral equation has to be extended far up- and downstream (to approximate infinity), as at least 10 airfoil chords as numerical tests have shown.

Applying this panel technique to the above equation yields a corresponding system of linear algebraic equations, where now the above aerodynamic influence functions are expressed by aerodynamic influence coefficient matrices (results of integration along one panel), and where *w*, $\delta\phi$, *f*, *g* are now column vectors of the corresponding values at the airfoil and at the tunnel walls. For the special cases of solid and open walls, the equations simplify to a closed form from which the (wall-affected) dipole strength, and hence the related unsteady pressures, can be calculated for a prescribed downwash *w*, i.e. oscillatory motion of the model.

$$\begin{aligned} &solid \quad walls \quad g = 0 \rightarrow w = \left(A + A_1 B_0^{(-1)} B\right)\delta\varphi \\ &open \quad walls \quad f = 0 \rightarrow w = \left(A + A_2 C_0^{(-1)} C\right)\delta\varphi \end{aligned} \tag{9.37}$$

For ventilated walls the boundary conditions outlined in chapter 2.3 have to be applied. Their implementation combines f, g, and $\partial f/\partial x$. If pressures on the walls are measured, f can be obtained by integrating (9.9) - see also (9.39) below - and then directly used in (9.36). In **Figures 16, 17** some typical results obtained from the described numerical method are illustrated. **Figure 16** shows the wall-influenced and the free-air unsteady pressure jumps in terms of the non-dimensional complex pressure coefficient $c_p = \left(p_{upper} - p_{lower}\right)/\left(q\,\Delta\alpha\right)$, with *q* = freestream dynamic pressure and $\Delta\alpha$ = amplitude, on a 2D plate performing pitching oscillations about a 42.5% chord axis, Mach number = 0.866, reduced frequency *k* = 0.050 and a wall distance b/L = 5. Solid walls increase the loads, while open walls produce the opposite effect. The results of **Figure 17** are obtained for the same conditions, except that the

reduced frequency has been changed to k = 0.182, which is close to the first solid wall resonance frequency. Now both the real and imaginary part are nearly zero.

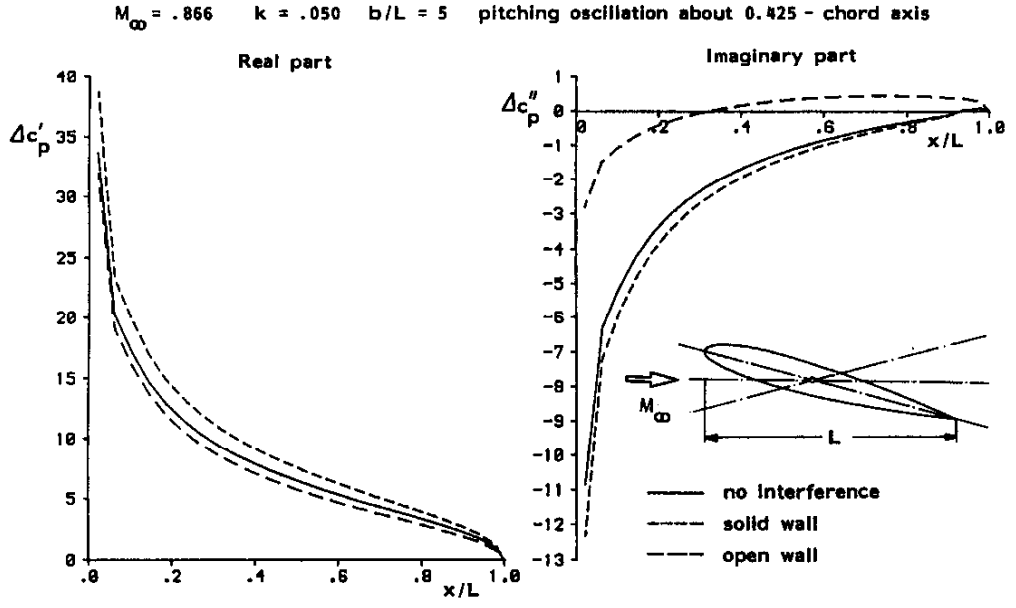

Figure 16 : Unsteady pressure around an oscillating airfoil with different tunnel wall conditions, far from tunnel resonance condition

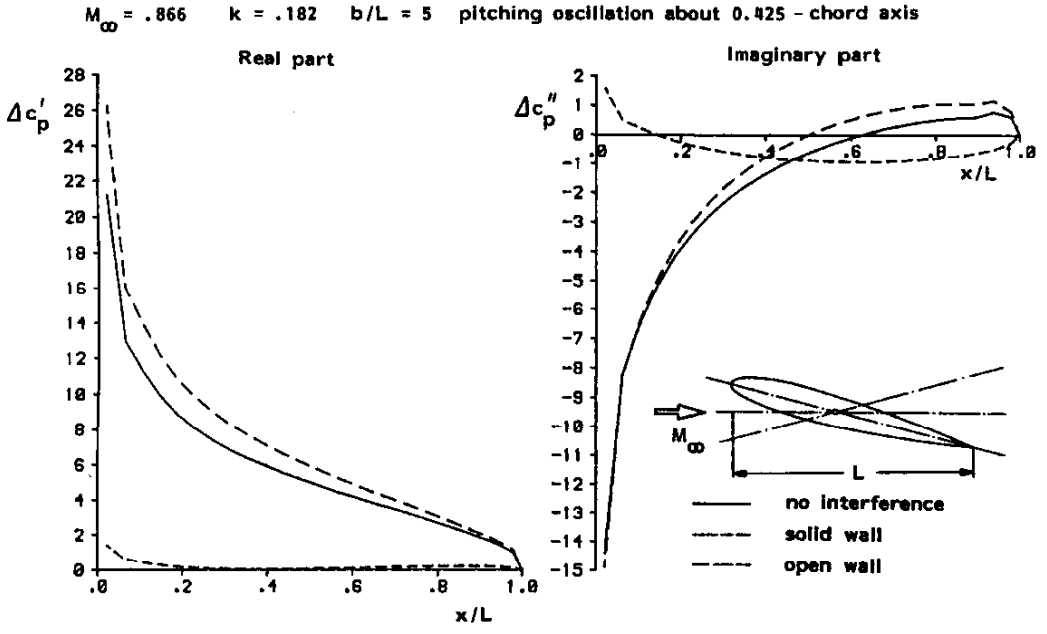

Figure 17 : Unsteady pressure around an oscillating airfoil with different tunnel wall conditions, close to tunnel resonance

The corresponding integrated unsteady lift values are shown in **Figure 18**. The overall agreement of the results with those of the analytical method of Fromme and Golberg, see **Figure 13** is good. The main discrepancy appears near the resonance frequencies, where the numerical panel method does not precisely predict the drop of magnitude to zero and produces oscillatory behaviour. The reason for this lies in the sensitivity of the numerical method with respect to modelling of the tunnel walls. These are modelled to be infinitely extended in the analytical method, while the panel method models only a finite extension (typically 10 - 100 chords).

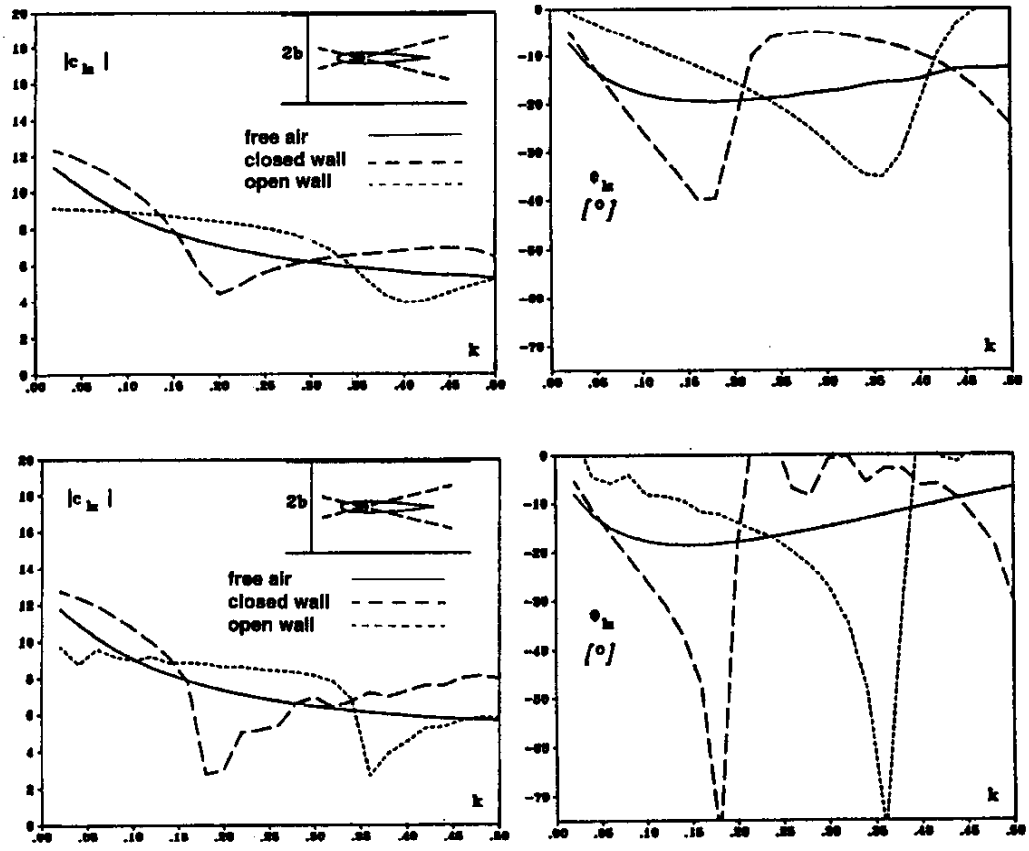

Figure 18 : Magnitude and phase of unsteady lift coefficient obtained by the linear panel method (same parameters as in Fig. 13)

Of course, unsteady aerodynamic predictions with wind tunnel wall effects can be obtained by other numerical methods as well. Today, the more sophisticated CFD-methods, which model the whole flow field and are based on non-linear equations, have also become a reliable tool in unsteady aerodynamics and they are easily applicable for the whole flow speed regime. **Figure 19** presents results for the test case of **Figure 17**, which have been obtained by one of the simplest CFD methods, based on the non-linear Transonic Small Perturbation (TSP) equation in the time domain, see [Voß 1990].

The unsteady results are obtained by solving the non-linear 2D TSP equations

$$\frac{\partial}{\partial x}\left(\beta^2\phi_x - \frac{(\gamma+1)}{2}M_\infty^2\phi_x^2\right) + \frac{\partial}{\partial y}\left(\phi_y\right) - \frac{\partial}{\partial t}\left(M_\infty^2\left(2\phi_x + \phi_t\right)\right) = 0 \qquad (9.38)$$

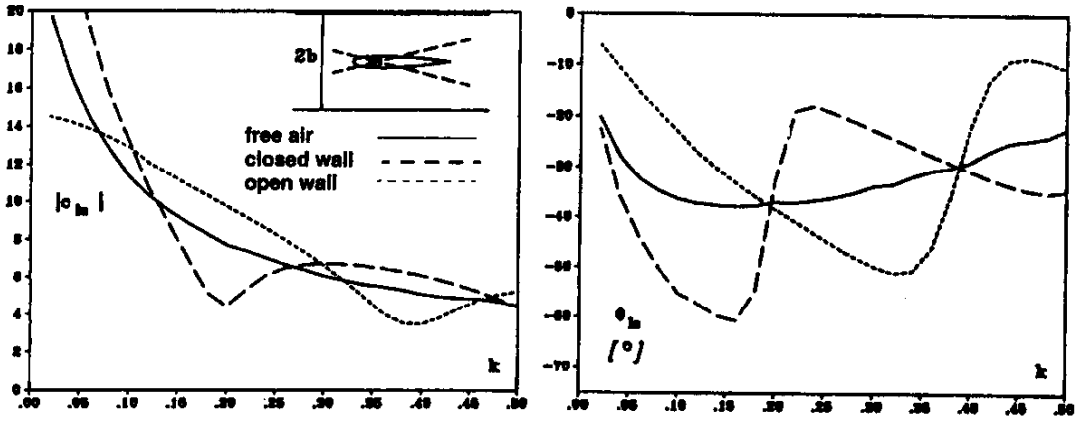

Figure 19 : Magnitude and phase of unsteady lift coefficient obtained by the TSP method (same parameters as in Figs. 13 and 18, $Ma_\infty = 0.866$, b = 5, pitching around a 50% chord, NACA 0006 airfoil).
upper : linear simulation lower : non-linear transonic simulation

The unsteady results are obtained by Fourier analysis from the complete time-dependent flow field simulation. In its upper part, **Figure 19** presents linear results, which are directly compatible with those of the panel method. Linear theory was simulated by neglecting the non-linear term in the above equation. An overall agreement with the results of the panel method and the exact analytical method appears, but the strong jumps of magnitude and phase values at resonance frequencies are smeared, and the values of the corresponding sharp peaks (magnitude: zero, phase angle: -90 degrees) are not captured very well. Outside of the resonance frequencies the agreement is very good, and there are no oscillations. The corresponding transonic results in the lower part show that the effects of unsteady tunnel interference are very similar to the linear behaviour. The underlying acoustic effects are only altered in transonic flow. Resonance appears for the same frequencies, the wall effects on phase angles are even stronger for transonic than for subsonic flow. The increased values of magnitude are due to the transonic effects.

A similar behaviour has been investigated for 3D transonic flows, see [35]. In 3D flows the same tendencies appear as in 2D, especially the resonance frequencies are observed for the same values. These investigations were carried out for rectangular wings in transonic flows. The unsteady interference effects for the rectangular wing are as big as those for the 2D airfoil. **Figure 20** shows results for a rectangular wing oscillating in pitch, with an extremely large value of the ratio between tunnel width and wing chord of 21.2. In general, one should expect that unsteady interference effects for 3D flows are smaller than for 2D flows. A general investigation of swept wings has not been done yet.

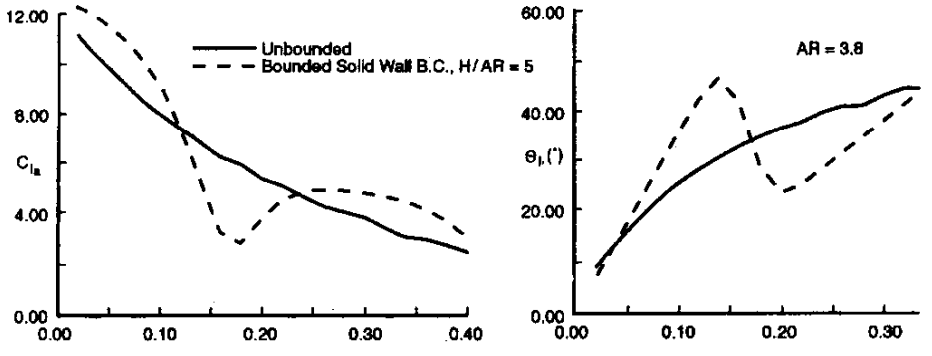

Figure 20 : Magnitude and phase of unsteady lift coefficient obtained by non-linear 3D TSP computation for a rectangular wing in a wind tunnel. (adapted from Seebass)

9.5 REDUCTION AND CORRECTION OF UNSTEADY WIND TUNNEL WALL INTERFERENCES.

9.5.1 UNSTEADY WIND TUNNEL WALL CORRECTIONS BY ANALYTICAL METHODS

In an early attempt, Jones [17] formulated a 2D correction technique, using an infinite series of image singularity distributions to model the tunnel wall effects. Similarly, Garner et al [14] developed a 3D correction method for ventilated tunnel walls by describing the wall influences through an infinite series of images of vortex distributions representing the model. This method has been modified by Kuczka, [18], for closed walls. Details can be found in the references. The applicability was demonstrated by computing unsteady tunnel wall pressure distributions by this analytical model and comparing them with corresponding test results. The agreements are very satisfying, even in transonic 3D flows at high incidences of the model. But the method is restricted to models of low aspect ratio and to low reduced frequencies (nearly quasi steady behaviour). The method was applied for the SDM model in wind tunnels with both a quadratic ventilated test section and a circular closed but stationary adaptive section. Due to the low frequencies, both the steady adapted closed walls and the ventilated walls provided results for the real part of unsteady lift and moment coefficients at the model with only a small remaining difference. This remaining unsteady interference can be corrected by Kuczka's method. **Figure 21a** shows that the correction method for unsteady interferences yields a slight shift of the real part of lift in a way that the corrected results of the different tunnels agree very well. The correction of the imaginary part is not as satisfactory. The corrected final results of both tunnels agree well only for low incidences; see **Figure 21b**. Nevertheless, this method should be further improved because it is simple and has the advantage that no precise knowledge about the model geometry and its motion are necessary - the measured wall-affected lift and moment coefficients are sufficient. General unsteady wall correction methods without restrictions with respect to model geometry and frequency need to take into account unsteady results measured at the tunnel walls.

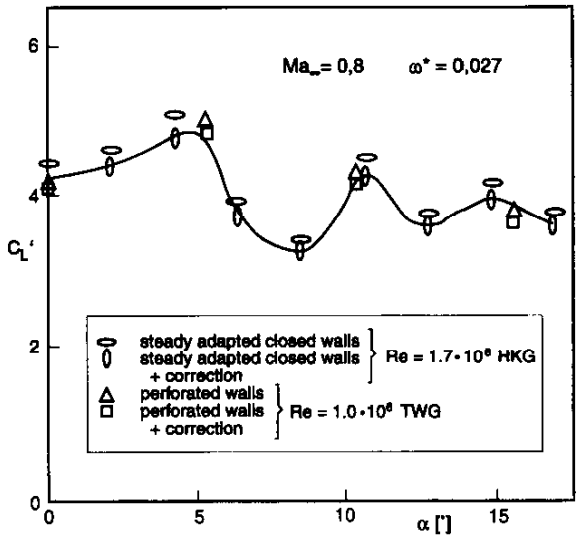

Figure 21a

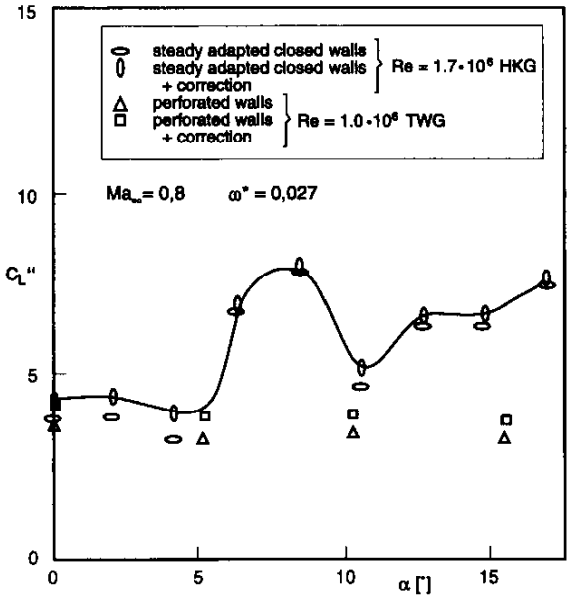

Figure 21b :

Unsteady in-phase and out-of-phase lift coefficients CL' and CL'' versus incidence for the SMD model tested in 2 wind tunnels and corrected for tunnel interference (adapted from Kuczka)

9.5.2 UNSTEADY WIND TUNNEL WALL CORRECTIONS USING MEASURED TUNNEL WALL PRESSURE VALUES AND NUMERICAL METHODS

9.5.2.1 DIRECT COMPUTATION OF THE TUNNEL WALL PROBLEM BY PANEL METHODS

If it is possible to measure the unsteady wall pressure distributions during the test, they can be used to correct the wall-influenced unsteady pressure data at the model to corresponding free air results. Such wall pressure measurements are a basic feature for steady flow adaptive wall concepts. For unsteady corrections both magnitude and phase of unsteady pressure have to be measured at a sufficient number of tunnel wall control points. These may serve for tunnel wall correction methods based on numerical unsteady aerodynamic methods. In [39] such methods for small amplitude oscillating models, based on the above panel method, are described and outlined in the following. As outlined in formula (9.9), the corresponding values of the velocity potential can be obtained from a measured unsteady (harmonic) tunnel wall pressure distribution c_p^w by the integration

$$c_p^w = -2\left\{\varphi_{\bar{x}}^w + i\frac{k}{\beta^2}\varphi^w\right\}e^{i\bar{x}} \quad \rightarrow \varphi^w = -\frac{1}{2}\int_{-\infty}^{\bar{x}} c_p^w(\bar{\zeta})\,\exp\left[i\left(k\bar{\zeta} - \frac{k}{\beta^2}\right)\bar{x}\right]d\bar{\zeta} \tag{9.39}$$

The wall pressures have to be measured at a sufficient number of control points distributed on the tunnel walls, including the regions upstream and downstream of the model. Then one obtains an integral equation for the wall-affected dipole distribution on the model by application of Green's method to the wind tunnel wall bounded flow control volume. The final equation reads as:

$$\left(A + A_2\, C_0^{(-1)} C\right)\delta\tilde{\varphi} = w - \left(A_1 + A_2\, C_0^{(-1)} C_1\right)\varphi^w \tag{9.40}$$

Here $\delta\,\varphi$ denotes the dipole strength for the wall-affected pressure on the airfoil. It can be seen that the wall interference effects change both the downwash and the kernel of the integral equation, compared to the free air equation $w = A\delta\,\varphi$. Substitution finally yields the following equation :

$$\tilde{A}_1\,\delta\tilde{\varphi} = \left(w - \tilde{A}_2\varphi^w\right) \quad with \quad A\delta\varphi = w \quad follows \quad \tilde{A}_1\,\delta\tilde{\varphi} = A\delta\varphi - \tilde{A}_2\varphi^w \tag{9.41}$$

Here the kernels (influence coefficient matrices) are known from theory and depend on model geometry, Mach number and reduced frequency. An extension to 3D problems is straightforward. For 3D cases Green's function is an exponential function instead of the Hankel function for 2D cases, and integration's have to be performed along the contour surfaces of tunnel walls, model and wake surface instead of lines. In the framework of the small disturbance approach, 3D models may be represented by panelling the projection area in the plane of streamwise and spanwise co-ordinate axes (parallel to upper and lower tunnel walls). With this method, no further information on the type of tunnel walls or model motion is needed, but the model geometry has to be represented by panels.

The 2D correction method of Sawada [34] uses Green's theorem as well, and is similar to the above approach. The advantage of his approach is that that pressure distributions appear directly in the integral equations, but integral kernels are rather complicated functions and extension to 3D will be very complicated. The results he obtained are encouraging for low frequencies and less satisfactory in the vicinity of resonance frequencies.

Extension of the described correction methods to transonic flows demands the reformulation of the integral equations based on an inhomogeneous Helmholtz equation, which can be derived from Eq. (9.2). Direct integral equation methods for the solution of 2D and 3D unsteady transonic flows under free air conditions and based on this approach are described in [16] and in [37]. The methods require the

computation of several additional kernel functions in order to model the transonic effects of the steady base flow field and for the inclusion of field sources in those parts of the flow field near local supersonic regions. **Figure 22** shows the control volume for these so-called field panel methods. These additional operators thus depend on the Mach number, reduced frequency, model geometry and steady flow, which would significantly complicate the procedure.

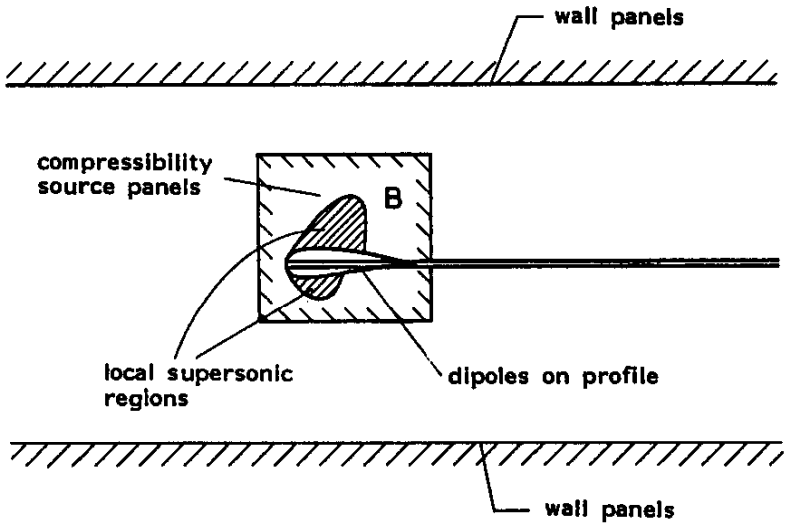

Figure 22 : Region of integration for the solution of transonic boundary value problem including the additional transonic near-field control area B

The corresponding integral equation for the correction values $\delta\varphi^c$ and φ^c of the dipole strength on the airfoil and of the potential values in the field

$$\delta\varphi^c = \delta\tilde{\varphi} - \delta\varphi \quad and \quad \varphi^c = \tilde{\varphi} - \varphi \tag{9.42}$$

involving the right-hand-side S of the basic nonhomogeneous Helmholtz equation and the potential values φ^w on the tunnel walls reads:

$$\int_0^\infty \delta\varphi^c \psi_{\bar{\eta}\bar{\eta}}\, d\zeta - \int\int_B S(\varphi^c)\psi_{\bar{\eta}}\, dF - \int_{-\infty}^\infty \varphi^w \psi_{\bar{\eta}\bar{\eta}}\, d\zeta = 0 \qquad airfoil \tag{9.43}$$

$$\int_0^\infty \delta\varphi^c \psi_{\bar{\eta}}\, d\zeta - \int\int_B S(\varphi^c)\psi\, dF - \int_{-\infty}^\infty \varphi^w \psi_{\bar{\eta}}\, d\zeta = -\varphi^c \quad in\ the\ field$$

9.5.2.2 SOLUTION FOR THE CORRECTION POTENTIAL BY PANEL METHODS

A slightly different approach is more promising. The method assumes closed adaptive tunnel walls which are adapted for the steady flow. Thus only the unsteady acoustic interferences will be corrected. A further assumption is that the component of the flow field which is caused by wall interference may be described by the linear theory. This is justified by the discussions in chapter 2.1. Thus the difference between velocity potential of the wall-affected tunnel flow and the desired value of the corresponding free air conditions fulfils the Helmholtz equation, and the correction value of the dipole strength and thus the airfoil pressure distribution is directly computed.

$$\varphi^c_{\bar{x}\bar{x}} + \varphi^c{}_{\bar{y}\bar{y}} + \lambda^2\varphi^c = 0 \tag{9.44}$$

$$\varphi^c = \tilde{\varphi} - \varphi$$

The corresponding boundary conditions are obtained by subtracting those of the wind tunnel flow (vanishing normal flow velocity on both the model surface and on the tunnel walls) from the free air conditions (nonreflecting far field conditions at the locations of the tunnel walls). The model surface conditions are prescribed by the oscillatory motion and are the same with and without tunnel walls, thus yielding

$$\varphi_{\bar{y}}^{c} = 0 \ (profile) \tag{9.45}$$

Nonreflecting far field conditions have been derived by different authors, see for example [20], or [9], for unsteady CFD methods, and they are applied here in their harmonic, time-dependent complex form, for the upper and lower walls, respectively

$$\left(\phi_x \pm \frac{M_\infty}{\sqrt{1 - M_\infty^2}} \phi_t \right) = 0 \tag{9.46}$$

Application at the tunnel wall locations, together with the potential transformation and subtracting from this the condition for solid tunnel walls (vanishing y-components of disturbance velocity) yields

$$\varphi_{\bar{y}}^{c} \pm \chi \varphi^{c} = \chi f^{w} \tag{9.47}$$

for the upper and lower walls, respectively with f denoting the value of the potential on the upper or lower wall and with

$$\chi = \frac{ik\, M_\infty}{\left(1 - M_\infty^2\right)} \tag{9.48}$$

The value of the velocity potential at the walls may be obtained from the measured wall pressures by integration as described above. Applying the notation of the preceding chapter yields

$$w^{c} = 0 \quad g^{c} \pm \chi f^{c} = \pm \chi f^{w} \tag{9.49}$$

and, finally, after some rearrangements, an integral equation for an unknown dipole distribution from which the pressure correction of the wall interference is obtained in the usual way, for details see [39]

$$\left(A + A_3 B\right) \delta\varphi^{c} = -\left(A_3 \tilde{B}_1 \pm \tilde{A}_2\right) \chi f^{w} \tag{9.50}$$

for the upper and lower walls respectively. **Figure 23** shows a result of this correction method for an unsteady transonic flow also including shock waves. Due to the non-existence of detailed unsteady transonic flow pressure measurements at the tunnel walls, this demonstration did not apply wind tunnel data,

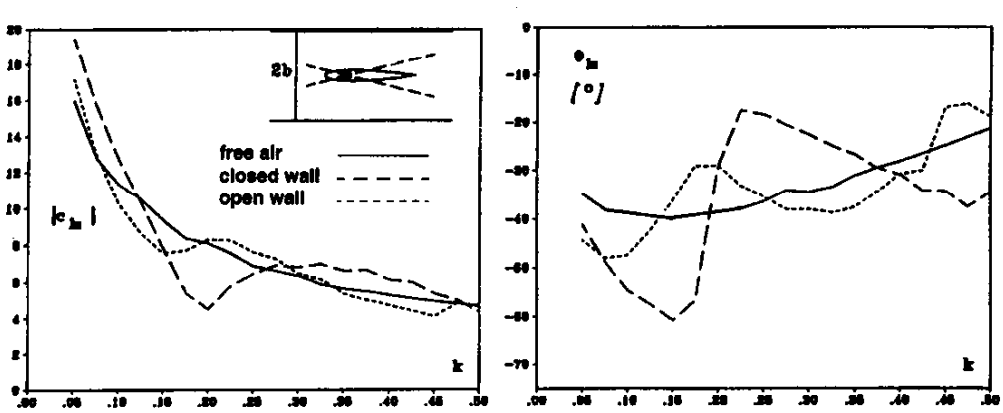

Figure 23 : Correction of unsteady tunnel wall interference in transonic flow
(NACA 0006, $Ma_w = 0.866$, b = 5, pitching around a 25% chord).

but CFD results were computed by the above-mentioned TSP method for the wind tunnel flow with closed walls and for free air condition. Both the results on the airfoil and at the walls were used as "experimental" results and were corrected in the described manner. The correction shows significant improvements of the wind tunnel simulation results towards free air simulated results, although the agreement of corrected and free air methods is still unsatisfactory - not only near the tunnel resonance. Especially phase angles should be accurate within a range of ± 5 degrees. But one has to keep in mind that the correction procedure is based on a linear formulation, while both the wind tunnel flow and the free flow include large non-linear effects.

References

[1] Acum, W.E.A., A Simplified Approach to the Phenomenon of Wind Tunnel resonance. ARC R&M 3371 (1962)

[2] Ashill, P.R., Keating, R.F.A., Calculation of Tunnel Wall Interference from Wall Pressure Measurements. RAE TR 85086 (1985).

[3] Bergh, H., Zwaan, R., Present Status of Unsteady Aerodynamics for Lifting Surfaces. AGARD CP 46 (1970)

[4] Beyers, M.E., Unsteady Wind-Tunnel Interference in Aircraft Dynamic Experiments. J. Aircraft, Vol. 29 (1992), pp. 1122-1129.

[5] Bland, S.R., The Two-Dimensional Oscillating Airfoil in a Wind Tunnel in Subsonic Flow. SIAM J. Appl. Math., Vol. 18, (1970), pp.830-848.

[6] Chang, Byeong-Hee, Sung, Bongzoo, Chang, Keun-Shik., Unsteady Adaptive Wall Models for Wind Tunnel Testing. AIAA J., Vol. 33 (1995), pp. 1536-1538.

[7] Cheung, C.W., Hancock, G.J. Wind Tunnel interference on Unsteady Two-Dimensional Airfoil Motions in Low Speed Flows. Aeronautical Journal, March 1988, pp.115-121.

[8] Davis, J.A., Transonic Interference effects in Testing of Oscillating Airfoils, Dissertation Ohio State University (1982)

[9] Engquist, B., Majda, A. Radiation Boundary condition for Acoustic and Elastic Wave Calculations. Comm. Pure and Appl. Math., Vol. 32 (1979) pp. 313-357.

[10] Försching, H., Voß, R., Adaption for Unsteady Flow, in "Adaptive Wind Tunnel Walls : Technology and Application", AGARD AR 269 (1990)

[11] Fromme, J.A., Golberg, M.A., Unsteady Two-Dimensional Airloads Acting on Oscillating Thin Airfoils in Subsonic Ventilated Wind Tunnels. NASA CR 2967 (1978)

[12] Fromme, J.A., Golberg, M.A., Aerodynamic Interference Effects on Oscillating Airfoils with Controls in Ventilated Wind Tunnels. AIAA J., Vol. 18 (1980), pp.417-426.

[13] Fromme, J.A., Golberg, M.A., Reformulation of Possio's kernel with Application to Unsteady Wind Tunnel Interference. AIAA J., Vol. 18 (1980), pp.951-957.

[14] Garner, H.C., The Theory of Interference Effects on Dynamic Measurements in Slotted-Wall Tunnels at Subsonic Speeds and Comparisons with Experiment. ARC R&M 3500 (1968).

[15] Garner, H.C., Theoretical Use of variable Porosity in Slotted Tunnels for Minimizing Wall Interference on Dynamic Measurements. ARC R&M 3706 (1971).

[16] Geißler, W., Voß, R., Investigations of the Unsteady Airloads with Oscillating Control in Sub- and Transonic Flows, in Proc. 1st Int. Symp. on Aeroelasticity, DGLR Report 82-01 (1982).

[17] Jones, M.A., Wind Tunnel Wall Interference Effects on Oscillating Airfoils in Subsonic Flow. ARC R&M 2943 (1953).

[18] Kuczka, D., Hybridverfahren für instationäre Messungen in transsonischen Windkanälen am Beispiel der harmonischen Nickschwingung. DFVLR-FB 88-19 (1988).

[19] Kong, L., Parkinson, G.V., Unsteady Flow testing in a Passive Low-Correction Wind Tunnel. In Wall Interference, Support Interference and Flow Field Measurements, AGARD CP 535 (1994), pp. 22-1-22-7.

[20] Kwak, D., Non-Reflective Far Field Boundary Conditions for Unsteady transonic Flow Computation. AIAA J., Vol. 19 (1981), pp.1401-1407.

[21] Lambourne, N., Destuynder, R., Kienappel, K., Roos, R., Comparative Measurements in Four European Wind Tunnels of the Unsteady Pressures on an Oscillating Model (The NORA Experiments). AGARD Report No. 673 (1980)

[22] Lambourne, N., Wind Tunnel Wall Interference in Unsteady Transonic Testing. AGARD VKI Lecture Series 1981-4 (1981)

[23] Landahl, M.T., Unsteady Transonic Flow. Pergamon Press (1969)

[24] Laschka, B., Wegner, W., Theoretische Behandlung der Böensimulation im Windkanal, ZFW 10 (1986), pp.168-173.

[25] Lu, Qizheng, Li, Qing, Lu, Bo., Experimental Investigation on the Interference effect of FL-23 Wind Tunnel Wall on Transonic Flutter. Acta Aerodynamica Sinica, Vol. 7 (1989, pp. 351-357.

[26] Mabey, D.G., The Reduction of Dynamic Interference by Sound-Absorbing Walls in the RAE 3 ft. Wind Tunnel. RAE TR 77120 (1977).

[27] Mabey, D.G., Resonance Frequencies of Ventilated Wind Tunnels. AIAA J., Vol. 18 (1980), pp.7-8.

[28] Mokry, M., Chan, Y.Y., Jones, D.J., Two-Dimensional Wind Tunnel Wall Interference. Chapter 8. Unsteady Wall Interferences. AGARDograph No. 281 (1983), pp.131-158.

[29] Moore, A.W., Wight, K.C., An Experimental Investigation of Wind Tunnel Wall Conditions for Interference-Free Dynamic Measurements. ARC R&M 3715 (1969).

[30] Platzer, M.F., Wind Tunnel Interference on Oscillating Airfoils in Low Supersonic Flow. Acta Mechanica, Vol. 16 (1973), pp.115-126.

[31] Possio, C., L'azione aerodinamica sul profilo oscillante in un fluido compressibile a velocita iposonara. L'Aerotchnica, Vol 18 (1938), pp. 441-458.

[32] Runyan, H.L., Watkins, C.E., Consideration on the Effect of Wind Tunnel Walls on Oscillating Air Forces for Two-Dimensional Subsonic Compressible Flows. NACA Report 1150 (1951).

[33] Runyan, H.L., Woolston, D.S., Rainey, A.G. Theoretical and Experimental Investigations of the Effect of Tunnel Walls on the Forces on an Oscillating Airfoil in Two-Dimensional Subsonic Compressible Flow. NACA Report 1262 (1955).

[34] Sawada, H., A New Method of Estimating Wind Tunnel Wall Interference in Unsteady Two-Dimensional Flow. NRC No. 21274 (1983).

[35] Seebass, A.R., Fung, K.Y., Przybytkowski, S.M., Advances in the Understanding and Computation of Unsteady Transonic Flow, in "Recent Advances in Aerodynamics", Springer (1983)

[36] Vogt, U., Computation of Unsteady Wind Tunnel Wall Influences on Pressure Distributions of Oscillating Airfoils, DFVLR IB 232-85 J15 (in German) (1985)

[37] Voß, R., Calculation of Unsteady transonic Flow about Oscillating Wings by a Field Panel Method, in Panel Method in Fluid Mechanics with Emphasis on Aerodynamics, Notes on Numerical Fluid Mechanics, Vol. 21 (1988), pp. 232-242.

[38] Voß, R., Über die Ausbreitung akustischer Störungen in transsonischen Strömungsfeldern von Tragflügeln, DFVLR-FB 88-13 (1988).

[39] Voß, R., Instationäre Windkanalwand-Interferenzen bei sub- und transsonischer Stömung, in Festschrift on the 60th birthday of Prof. H.W. Förscher. DLR Institute of Aeroelasticity (1990), pp. 169-185.